Thiacrown Ether Substituted Styryl Dyes: Synthesis, Complex Formation and Multiphotochromic Properties

Olga A. Fedorova, Yuri V. Fedorov,* Artem I. Vedernikov, Sergey P. Gromov, Olga V. Yescheulova, and Michael V. Alfimov

Photochemistry Center of Russian Academy of Sciences, Novatorov str., 7a, 117421, Moscow, Russia

M. Woerner, Stefan Bossmann, and Andre Braun

Engler-Bunte-Institut, Universität Karlsruhe (TH), Richard-Willstär-Allee 5, 76128 Karlsruhe, Germany

Jack Saltiel*

Department of Chemistry and Biochemistry, The Florida State University, Tallahassee, Florida 32306-4390

Received: November 30, 2001; In Final Form: April 11, 2002

Syntheses of two series of new styryl dyes incorporating thiacrown ether moieties (CSDs **3a**−**e**, **4a**−**e**) are described. ^{1}H NMR and UV−vis measurements show that these compounds exhibit a strong preference for formation of complexes with heavy metal ions. Polarographic measurements allow conversion of relative complex formation stability constants, determined spectrophotometrically, into absolute values. The photochromic properties of the CSDs are based on reversible trans-cis isomerization and [2+2]-photocycloaddition. The influences of the terminal group of the *N*-substituent and of the size and composition of the crown ether cavity on metal cation complexation selectivity and on photochromism are evaluated.

Introduction

Cyanine dyes exhibiting photoswitching properties are central to a vigorously developing field of research.[1,2] Crown ether substituted dyes that absorb light in the visible region of the spectrum and bind metal cations selectively,[3−7] have been used, for example, as reagents for calorimetric or fluorimetric metal cation determinations, as components of photoswitchable molecular devices,[8,9] as photosensitizers in photographic chemistry,[10] and as photoelectric materials.[11] Photoisomerization and complexation-induced photochromic responses of such cyanine and merocyanine dyes provide additional dimensions that may lead to advantageous applications in materials science.[12,13]

Incorporation of the benzodithia-18-crown-6 ether moiety into novel styryl dyes was facilitated by improved synthetic approaches to formyl derivatives of the crown ethers.[14−18] In combination with the proper chromophore the metal ion selectivity of such dyes is enhanced or modulated by the absorption of light. Specifically, the benzodithia-18-crown-6 styryl dye **4c** is rendered 11 times more selective for Hg^{2+} upon trans-cis photoisomerization.[19] One or more sulfur atoms have been incorporated into a variety of macrocycles, including crown ethers,[20] cryptates,[21] cyclophanes,[22] and other shape-specific ligands.[23] However, the synthesis of multifunctional systems containing benzothiacrown ether moieties has remained a challenge.

This work concerns the syntheses and photochromic properties of benzothiacrown ethers of the benzothiazolium family (crown ether-containing styryl dyes, CSDs **3a**−**e**, **4a**−**e**, Scheme 1). The effects of the identity of the metal cation, the nature of the terminal group on the *N*-substituent, and the size and composition of the thiacrown ether cavity of the CSDs are evaluated. Depending on these factors, these compounds exhibit metal ion sensitive photochromic transformations based on *E*−*Z*-photoisomerization and [2+2]-photocycloaddition.

Results

Synthesis. The syntheses of CSDs **3c and 4c** were described previously.[15−19] Condensation of *N*-substituted benzothiazolium salts **1a**,**b** with 4′-formylbenzothiacrown ethers **2a**,**b**,**d**,**e** in the presence of pyridine (Scheme 1), following the procedure described in ref 19, yielded CSDs **3a**,**b**,**d**,**e** and CSDs **4a**,**b**,**d**,**e**. Structural identifications of CSDs **3a**,**b**,**d**,**e** and **4a**,**b**,**d**,**e** were based on their ^{1}H NMR spectra (see below and the Experimental Section) and are consistent with the results of elemental analyses. Assignment of *E* configurations to **3a**,**b**,**d**,**e** and **4a**,**b**,**d**,**e** was on the basis of the spin−spin coupling constant for the olefinic protons, $^3J_{trans} = 15.6$ Hz.

Complex Formation and Equilibrium Constant Determinations. Complex formation of **3c** and **4c** with $Pb(ClO_4)_2$ was studied by spectrophotometric titration. In direct experiments, the ratio of **3c** to $Pb(ClO_4)_2$ was varied by adding aliquots of a solution containing known concentrations of **3c** and of $Pb(ClO_4)_2$ to a solution of **3c** alone of the same concentration. The absorption spectrum of each solution was recorded and the stability constant of the complex was determined using the ≪Hyperquad≫ program, which applies a least squares approach in obtaining best fit equilibrium constant values from potentiometric and/or spectrophotometric data.[24] The stability constants of the complexes of (*E*)-**4c** and (*Z*)-**4c** with Pb^{2+} are too large for determination by direct spectrophotometry. They were determined indirectly by spectrophotometric titration with the competing ligand 2,3-benzo-1,10-dithia-18-crown-6 ether (BDT18C6), as previously described.[19] Aliquots of a solution

10.1021/jp014382m CCC: $22.00
Published on Web 06/04/2002

SCHEME 1

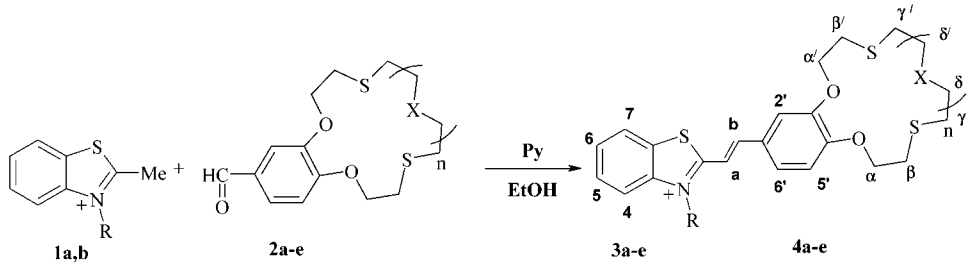

1a: R = Me (ClO_4-);
1b: R = $(CH_2)_4SO_3$-

2a: n = 0;
2b: n = 1, X = O;
2c: n = 2, X = O;
2d: n = 3, X = O;
2e: n = 2, X = S

R = Me (ClO_4-);
3a: n = 0;
3b: n = 1, X = O;
3c: n = 2, X = O;
3d: n = 3, X = O;
3e: n = 2, X = S

R = $(CH_2)_4SO_3$-
4a: n = 0;
4b: n = 1, X = O;
4c: n = 2, X = O;
4d: n = 3, X = O;
4e: n = 2, X = S

TABLE 1: Complexation Induced ^{1}H NMR Chemical Shift Changes in the Crown Ether Moiety in MeCN-d_3 at 50 °C ([CSD]:[M^{2+}] = 1:1)

		$\Delta\delta$, *ppm*				
CSD	M^{2+}	α,α′	*β*,*β*′	*γ*,*γ*′	*σ*,*σ*′	*ϵ*,*ϵ*′
E-**3a**	Hg^{2+}	−0.14	0.51	0.44		
	Pb^{2+}	0.14, −0.06	0.13	0.09		
E-**3b**	Hg^{2+}	0.26	0.78	0.70	0.22	
	Pb^{2+}	0.17	0.20	0.17	0.19	
	Cd^{2+}	0.01	0.03	0.03	0.01	
E-**3c**	Hg^{2+}	0.26	0.82	0.72	0.23	0.21
	Pb^{2+}	0.35	0.34	0.31	0.43	0.37
	Cd^{2+}	0.06	0.11	0.10	0.05	0.10
E-**3d**	Hg^{2+}	0.19	0.61	0.54	0.10	0.06 (H*θ* 0.06)
	Pb^{2+}	0.26, 0.19	0.38	0.32	0.43	0.28 (H*θ* 0.35)
E-**3e**	Pb^{2+}	0.19	0.48	0.46	0.42	0.42

TABLE 2: Equilibrium Constants for Pb^{2+} and Hg^{2+}Complex Formation with CSDs

complex	log *K*	complex	log *K*
(*E*)-**3b**·Hg^{2+}	15.9(1);[a] 15.7(1)[b]	(*E*)-**4b**·Hg^{2+}	18.0(1)[b]
(*E*)-**3c**·Hg^{2+}	18.2(1);[a] 18.0(1)[b]	(*E*)-**4c**·Hg^{2+}	19.8(1)[b,c]
(*E*)-**3c**·Pb^{2+}	5.61(2)[b]	(*E*)-**4c**·Pb^{2+}	7.57(3)[b]
(*E*)-**3e**·Hg^{2+}	21.0(1)[a]	(*E*)-**4e**·Hg^{2+}	20.7(1)[b]
BDT12C4·Hg^{2+}	22.7(2)[a,d]	(*Z*)-**4c**·Hg^{2+}	20.8(1)[b,c]
BDT15C5·Hg^{2+}	18.0(1)[a]	(*Z*)-**4c**·Pb^{2+}	8.75(3)[b]
BDT18C6·Hg^{2+}	19.5(1)[a,c]		
BDT18C6·Pb^{2+}	7.26(2)[b]		

[a] These values were determined polarographically for 0.01 M solution of Et_4NClO_4 in MeCN at 20 °C; values in parentheses are uncertainties in the last significant figure shown. [b] These values were determined spectrophotometrically in MeCN at 20 °C; values in parentheses are uncertainties in the last significant figure shown. [c] These values were taken from ref 19. [d] Stoichiometry of ligand to metal complex is 2:1.

containing BDT18C6, 2×10^{-3} M, were added to a solution containing known concentrations of **4c** and $Pb(ClO_4)_2$. Treatment of the absorption spectra of these solutions using the ≪Hyperquad≫ program[24] yielded the equilibrium constant between the two complexes. This equilibrium constant and the value of the stability constant of the BDT18C6/$Pb(ClO_4)_2$ complex were used to calculate the stability constant of the complex of **4c** with $Pb(ClO_4)_2$. The stability constant of the BDT18C6/$Pb(ClO_4)_2$ complex was based on results from the spectrophotometric titration of the **3c**/$Pb(ClO_4)_2$ complex with BDT18C6 as the competing ligand. Ionic strengths varied from 5×10^{-5} to 2×10^{-4} M, in the course of these titrations.

In the cases of (*E*)-**4c** complexation with Pb^{2+} and Hg^{2+}, formation of complexes having 2:2 CSD:M^{2+} stoichiometry is suggested by the observation of highly stereospecific metal ion mediated ligand dimerization (see below). Qualitative spectroscopic evidence for complexes of higher stoichiometry was obtained for the (*E*)-**4c**/Pb^{2+} system. UV−vis absorption spectra for a 10^3-fold range of (*E*)-**4c** concentrations (10^{-3}−10^{-6} M) are nearly identical [λ_{max} 414−417 nm and $\epsilon_{max} = (3.73 \pm 0.05) \times 10^4$ $M^{-1}cm^{-1}$] provided that an excess concentration of Pb^{2+} (2- to 10-fold) is employed. However, the λ_{max} of the LAB progressively shifts to shorter wavelengths as the concentration of equimolar (*E*)-**4c**/Pb^{2+} acetonitrile solutions and hence, the (*E*)-**4c**·Pb^{2+} concentration, is increased: λ_{max} = 432.4, 422.4, 416.9 and 416.5 nm for [(*E*)-**4c**] = [$Pb(ClO_4)_2$] = 2.0×10^{-6}, 1.0×10^{-5}, 1.0×10^{-4}, and 1.0×10^{-3} M, respectively. Because, on the basis of the equilibrium constant in Table 2, nearly all of the ligand is bound to Pb^{2+} for all of these equimolar solutions (89% at 2.0×10^{-6} M), the blue shift probably reflects further aggregation of the 1:1 complex. At low (*E*)-**4c**·Pb^{2+} concentrations aggregation probably favors 2:2 complex formation via stepwise associations between the crown ether bound Pb^{2+} and the alkyl sulfonate side chains in a bimolecular fashion, however, at higher concentrations (*E*)-**4c**·Pb^{2+} may interfere with the second step in dimer formation and divert the system toward higher linear aggregates. The effect of increasing [Pb^{2+}] is especially pronounced at low (*E*)-**4c** concentration. For instance, with [(*E*)-**4c**] = 2.0×10^{-6} M, increasing [$Pb(ClO_4)_2$] from 2.0×10^{-6} to 2.0×10^{-5} M shifts the λ_{max} of the LAB from 432.4 to 417 nm, consistent with the conclusions that (a) the 2:2 complex absorbs to the red of the 1:1 complex and (b) Pb^{2+} interferes with 2:2 complex formation. As will be shown below, these qualitative conclusions are consistent with the concentration dependence of photodimerization quantum yields (see Discussion, under Quantum Yield Interpretation).

Complex formation between benzodithia-12-crown-4 (BDT12C4), benzodithia-15-crown-5 (BDT15C5), benzodithia-18-crown-6 (BDT18C6), and the CSDs **3b**,**c**,**e** with $Hg(ClO_4)_2$ was studied by polarography. Acetonitrile solutions of BDT12C4, BDT15C5, and BDT18C6 and of the dyes **3b**,**c**,**e** in the presence of 0.1 M Et_4NClO_4 as supporting electrolyte, give well-defined mercury anodic waves when subjected to polarography at a dropping mercury electrode. In these measurements, the concentrations of BDT12C4, BDT15C5, and BDT18C6 were varied from 2×10^{-4} to 4×10^{-3} M and those of the dyes **3b**,**c**,**e** were varied from 2.5×10^{-4} to 1×10^{-3} M. The two electron reversible oxidation of mercury was confirmed by the 30 ± 4 mV half-width of the observed differential anodic wave. The oxidation of Hg to Hg^{2+} in the presence of each ligand is

TABLE 3: Photoisomerization and Photodimerization Quantum Yields of the Hg^{2+} and Pb^{2+} Complexes of CSDs (*E*)-4a−e[a]

complex	φ_{t-c}	φ_{c-t}	$10^4\varphi_{PCA}$
[(*E*)-**4a**]·Hg^{2+}	0.38	0.68	1.3
[(*E*)-**4b**]·Hg^{2+}	0.45	0.52	28
[(*E*)-**4c**]·Hg^{2+}	0.48	0.55	1.3
[(*E*)-**4c**]·Pb^{2+}	0.35	0.50	10
[(*E*)-**4d**]·Hg^{2+}	0.42	0.50	0.79
[(*E*)-**4e**]·Hg^{2+}	0.34	0.67	-

[a] Excitation intensity = 2.3×10^{-6} einstein/(s L); ligand concentrations were 4.0×10^{-5} M, and $Pb(ClO_4)_2$, and $Hg(ClO_4)_2$ concentrations were 7.0×10^{-5} and 4.1×10^{-5} M, respectively, in acetonitrile.

described by

$$Hg^{2+} + xL = HgL_x^{2+} + 2e^- \quad (1)$$

$$K = [HgL_x^{2+}]/\{[Hg^{2+}][L]^x\} \quad (2)$$

where L is the ligand and x gives the stoichiometry of the reaction. The desired equilibrium constant, $K = [(HgL_x)^{2+}]/\{[Hg^{2+}][L]^x\}$, for each ligand is related to the half-wave potential, $E_{1/2}$, of the solutions according to

$$E_{1/2} = E_0 - 0.0291\{\log K + \log [L/2]^{x-1} - \log [k_f/k_c]\} \quad (3)$$

where E_0 is the formal potential of the Hg/Hg^{2+} half-cell vs the Ag/(0.01 M $AgNO_3$) electrode and k_f and k_c, the diffusion rate constants of free and complexed ligand, respectively, are assumed to be identical. The difference between 1.120 V, the standard potential of the Hg/Hg^{2+} half-cell in acetonitrile vs the normal hydrogen electrode (NHE in water), and 0.548 V, the value for the Ag/(0.01 M $AgNO_3$) half-cell in acetonitrile vs NHE gives $E_0 = 0.572$ V.[25,26] $E_{1/2}$ values were found to be independent of [L] in all cases, with the exception of BDT12C4, establishing $x = 1$ (eq 3) consistent with the spectrophotometric observations. In the case of BDT12C4, $E_{1/2}$ values are linearly dependent on log [L/2] establishing $x = 2$ (eq 3). Table 2 shows the polarographically determined log K values.

Quantum Yields. As can be seen in Table 3, photoisomerization quantum yields far exceed the quantum yields of the photocycloaddition reactions. Accordingly, during the initial irradiation period, a photostationary mixture of *E*- and *Z*-isomers is attained prior to significant loss of complex to ligand photodimerization. Conversions to cyclobutane photocycloadduct (PCA) were determined from the decrease in complex concentration, which was based on the change in absorbance at the LAB maximum of the photostationary mixture of *E*- and *Z*-isomers, where the PCA does not absorb. Effective quantum yields for PCA formation were estimated from the slope of the plot of the complex concentration decrease vs the light intensity absorbed by the solution (I_{abs}) for conversions lower than 30%. I_{abs} in einstein·$L^{-1}$was calculated from: $I_{abs} = I_o(1-10^{-D(t)})t$, where $I_o = 5 \times 10^{-6}$ einstein·L^{-1}·s^{-1} is the incident light intensity, determined by ferrioxalate actinometry,[1] and $D(t)$ is the average absorbance of the solution, $0.5[D(t_2) + D(t_1)]$, assuming linear absorbance change for the $(t_2 - t_1)$ time interval. Due to a large difference between quantum yields of photoisomerization and photocycloaddition reactions the consumption of complex was negligible during photostationary state formation.

Effective PCA formation quantum yields were determined on excitation at 365 nm [light intensity = 0.507×10^{-8} einstein/(s cm^2)] of acetonitrile solutions containing several concentrations of **4c** and of $Pb(ClO_4)_2$. The results are given in Table 4. Although **4c** was initially present as the pure *E*-isomer, the solutions attain concentration dependent trans/cis photostationary states of the of **4c**/Pb^{2+} complexes (365 nm) well before significant losses, due to PCA formation, occur. Concentration dependent photostationary fractions of *c*-**4c** (f_{c-4c}) are based on the absorbance of *t*-**4c** at long wavelengths where only *t*-**4c** absorbs, Table 4.

TABLE 4: Concentration Effects on Photodimerization Quantum Yields of the 4c/Pb^{2+} System[a]

10^5 [**4c**][b], M	10^4 [$Pb(ClO_4)_2$], M	$10^3\varphi_{PCA}$	f_{c-4c}[c]
1.0	10	0.289	0.65
5.0	10	0.708	0.61
50	10	1.48	0.53
5.0	1.0	1.46	0.59
1.0	0.2	0.818	0.64
4.0	0.7	1.0[d]	

[a] Excitation at 365 nm, intensity = 5.0×10^{-6} Einstein/(s L). [b] Initial concentration of *E*-**4c** in acetonitrile. [c] Photostationary state fraction. [d] From Table 3.

Discussion

Complex Formation and Photoisomerization of the Cationic CSDs 3a−e. Addition of Hg^{2+}, Pb^{2+}, Cd^{2+}, Ni^{2+}, or Zn^{2+} perchlorates into (*E*)-**3a−e** solutions results in hypsochromic shifts of the long wavelength absorption bands (LABs), indicating formation of complexes (*E*)-**3a−e**·M^{2+} (Scheme 2). The long wavelength electronic transition in these CSD molecules involves displacement of electron density from the benzene ring to the heterocyclic moiety. The electron demand of a metal ion bound to the thiacrown ether moiety diminishes this effect and causes a hypsochromic shift of the LAB, whose magnitude depends on the identity of the metal ion. Relatively large LAB hypsochromic shifts (18−20 nm) are observed for **(***E***)-3a−e** in the presence of Hg^{2+} or Pb^{2+} in MeCN, whereas, corresponding shifts in the presence of Cd^{2+}, Zn^{2+}, or Ni^{2+} are much smaller (1−2 nm). The smaller LAB shifts for the complexes of Cd^{2+}, Zn^{2+}, and Ni^{2+} ions could be due to (a) small K values and/or to (b) formation of very strong M^{2+}/S bonds in the thiacrown ether cavities of the CSDs attenuating the interaction of the metal ion with the O atoms that are directly conjugated with the chromophore.

With the exception of the ^{1}H NMR spectrum of [(*E*)-**3e**]·Hg^{2+} in MeCN-d_3, which is difficult to interpret because of substantially broadened signals, the ^{1}H NMR spectra of the CSDs in this study and of their complexes with metal cations confirm the validity of the above structural assignments and interpretation. The weak complexing abilities of Zn^{2+} and Ni^{2+} ions is reflected in small changes in the ^{1}H NMR spectra when they are added to **3a−e**, and corresponding changes in the UV spectra are similarly small. However, on addition of Cd^{2+}, Hg^{2+}, or Pb^{2+} to MeCN-d_3 solutions of (*E*)-**3a−d** the entire ^{1}H NMR spectrum shifts downfield due to the association of the metal cations with the CSDs and the chemical shift changes, $\Delta\delta$, are most pronounced for the methylene hydrogen atoms of the crown ether moiety. Comparison of the $\Delta\delta$ values in MeCN-d_3 for these hydrogen atoms upon [(*E*)-**3a−d**]·M^{2+} complex formation is instructive (Table 1). Relatively uniform coordination contributions toward Pb^{2+} by oxygen and sulfur atoms in the crown ether moieties of (*E*)-**3a−e** are reflected in rather similar $\Delta\delta$ values for all methylene hydrogen atoms. The lack of coordination preference of Pb^{2+} between O and S is especially

SCHEME 2

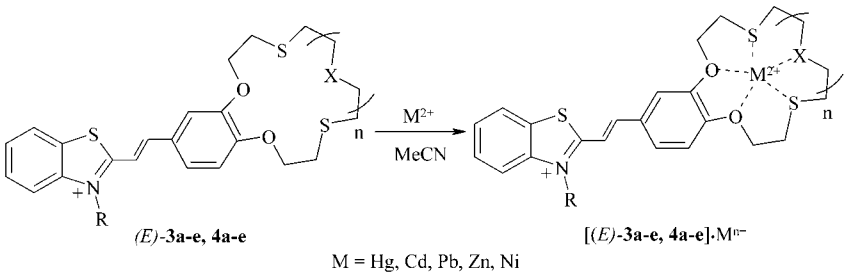

SCHEME 3

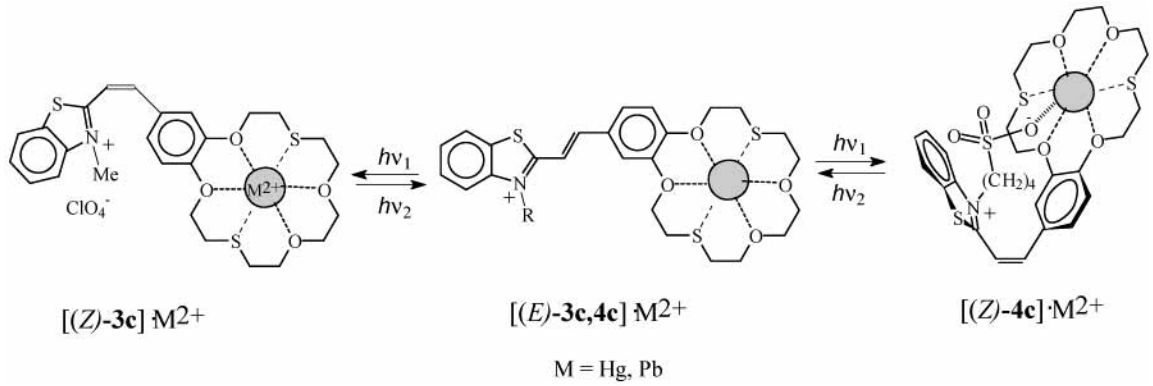

evident in very similar $\Delta\delta$ values for the methylene hydrogen atoms of **3c** and **3e**, which have different combinations of S and O atoms in nearly identical crown ether cavities. Preferential coordination of Hg^{2+} and Cd^{2+} metal cations by the S atoms in CSDs **3a**−**e** is reflected in relatively large $\Delta\delta$ values for methylene hydrogen atoms bonded to S. The preference of the dithiacrown ether moiety for the "softer" metal cations is seen in the generally larger $\Delta\delta$ values upon complex formation with Hg^{2+} instead of Cd^{2+}. Similarly, the difference in electron demand between Pb^{2+} and Hg^{2+} leads to smaller $\Delta\delta$ values for the Pb^{2+} complexes.

The strong binding between the four sulfur atoms in the crown ether cavity and the Hg^{2+} cation explains why the stability constant of [(*E*)-**3e**]·Hg^{2+} is higher than those for [(*E*)-**3a**−**d**]·Hg^{2+} in which only two sulfur atoms are available (Table 2). The overall binding strength of the dithiacrown ether compounds toward Hg^{2+} decreases in the order **3c** > **3b** > **3d** > **3a**, as compared with Pb^{2+} for which the order changes to **3c** ≅ **3e** ≅ **3d** > **3b** > **3a** (Table 1). The stronger coordination of Cd^{2+} with the crown ether moiety of (*E*)-**3c** than with the crown ether moiety of (*E*)-**3b** is similarly revealed by the more pronounced changes in the chemical shifts of the methylene hydrogen atoms (Table 1). The ^{1}H NMR results are consistent with the relative magnitude of stability constants obtained in the UV−vis studies (Table 2), namely, the log *K* values of complexes of the CSDs with a common metal cation, [(*E*)-**3a**−**e**]·Hg^{2+}, decrease in the order **3e** > **3c** > **3b**. The results can be explained on the basis of well-established empirical rules for predicting relative stability constants for complexes of metal cations with simple crown ethers. Ease of complex formation depends on (a) the size correlation between the crown ether cavity and the cation radius and (b) the nature and number of heteroatoms that participate in coordination with the metal cation. In the CSD series **3a**−**3d**, the size of the crown ether cavity and the number of oxygen atoms increase as *n* is increased with X = O, Scheme 1. Because all of these CSDs have only two S atoms in the crown ether moiety, the coordination preference of Hg^{2+} and Cd^{2+} for S over O atoms is expressed best when the size of the crown ether cavity best accommodates the size of the cation. On the basis of the nearly identical ionic radii of Hg^{2+} and Cd^{2+}, the size of the 18-crown-6 ether cavity in (*E*)-**3c** is expected to be most appropriate for each of these cations. Accordingly, the much larger preference of the thiacrown ether moiety for the "softer" metal cation, mentioned above, is especially evident in a comparison of the much larger $\Delta\delta$ values for the (*E*)-**3c**·Hg^{2+} complex than for the (*E*)-**3c**·Pb^{2+} complex, consistent with the large stability constants of the complexes of Hg^{2+} with (*E*)-**3c** and (*E*)-**4c**, Tables 1 and 2. The Pb^{2+} cation exhibits low, relatively uniform coordination abilities toward O and S atoms, accounting for the very low stability constant of the (*E*)-**3c**·Pb^{2+} complex, despite the optimum cavity/ionic radius fit.

The 2:1 stoichiometry of the complex between CSD **3a** and Hg^{2+}, [(*E*)-**3a**]$_2$·Hg^{2+}, was based on the end-point of the spectrophotometric titration and is reflected in the unusual upfield shift of the α hydrogen atoms of the complexed crown ether moiety.

Irradiation of acetonitrile solutions of (*E*)-**3a**−**e** or their complexes with $Hg^{2+}$and Pb^{2+} cations with 365 or 436 nm light leads to rapid changes in the absorption spectra due to reversible $E \leftrightarrows Z$ photoisomerization (Scheme 3). The absorption spectra of the *Z*-isomers of dyes **3a**−**e** and of their complexes with the Hg^{2+} cation were calculated by applying Fischer's method[27] using the corresponding spectra of the *E*-isomers and the spectra of photostationary states obtained upon irradiation with 365 and 436 nm light, as previously described.[19] The absorption spectra of the isomers **3c**, and of the isomeric complexes with Pb^{2+} are shown in Figure 1. The shapes of the spectra of the complexed isomers are remarkably similar to those of the corresponding uncomplexed isomers, the major effect of complexation being small LAB hypsochromic shifts of 21 and 27 nm for the *E* and *Z* isomers, respectively. Furthermore, the small change in the shift between *E* and *Z* isomers upon complexation with Pb^{2+} (13 nm uncomplexed, 19 nm complexed) reveals that complexation does not disturb the interaction of the conjugated moieties

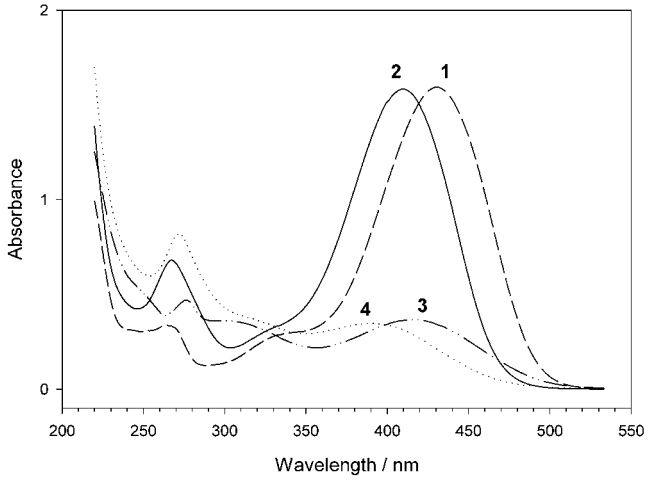

Figure 1. UV−vis absorption spectra of **3c** and of the complex of **3c** with $Pb(ClO_4)_2$ in MeCN ($C_L = 4 \times 10^{-5}$ M, $C_{Pb} = 7 \times 10^{-5}$ M): (*E*)-**3c** (1), [(*E*)-**3c**]·Pb^{2+} (2), (*Z*)-**3c** (3), [(*Z*)-**3c**]·Pb^{2+} (4).

in this CSD and, consequently, that complexation does not significantly alter the degree of planarity of the isomeric ligands (Scheme 3).

Complex Formation and Multiphotochromic Behavior of the Betaine CSDs 4a−e. The size compatibility between crown ether cavity and ionic radius is reflected in the stability constants for the complexes with Hg^{2+}, which decrease in the order **4e** > **4c** > **4b** (Table 2). As noted above, the same order applies in the [(*E*)-**3a**−**e**]·Hg^{2+}series of complexes. Comparison of the stability constant values K_E, (where K_E and K_Z are the stability constants for *E*- and *Z*-CSDs, respectively, see eq 2 with $x = 1$) for analogous complex pairs (*E*)-**4c**·Pb^{2+}/(*E*)-**3c**·Pb^{2+}, (*E*)-**4b**·Hg^{2+}/(*E*)-**3b**·Hg^{2+} and (*E*)-**4c**·Hg^{2+}/(*E*)-**3c**·Hg^{2+} reveals ratios of 91, 200, and 63, respectively. Introduction of the ω-alkylsulfonate substituent in the *E* isomers of the CSDs significantly enhances their ability to bind metal cations. No such stability constant enhancement by the remote ω-alkylsulfonate substituent would be expected if the 1:1 ligand to metal cation composition were strictly maintained in the (*E*)-**4a**−**d** complexes with Hg^{2+} or Pb^{2+} cations. Involvement of the ω-alkylsulfonate groups in the formation of complexes having higher stoichiometric compositions, e.g., dimeric (2:2 ligand to metal cation ratio) could account for the enhanced metal ion complexation ability. Analogous dimeric complexes have been observed on association of Mg^{2+} with related benzothiazole styryl dyes incorporating oxygen crown ether moieties.[28−31] Available data do not allow separate calculation of individual stability constants for 1:1, 2:2 and higher stoichiometry complexes. Accordingly, the log K_E values for the (*E*)-**4**·M^{2+} complexes in Table 2 should be regarded as effective values that include the neglected contributions of higher complexes.

^{1}H NMR spectroscopic observations provide independent experimental confirmation for dimeric complex formation. Direct determination of $\Delta\delta$ values upon complex formation between Pb^{2+} or Hg^{2+} and CSDs **4a**−**e** in MeCN-d_3 is not feasible because the free ligands are not sufficiently soluble in this solvent. Reliable estimates of $\Delta\delta$s were obtained with the use of (*E*)-**4c**·Mg^{2+} as reference. Coordination of Mg^{2+} with the sulfonate group in the dimeric complex increases the solubility of the CSD, without affecting the chemical shifts of the aromatic and crown ether methylene protons. The Pb^{2+} complexes were chosen for detailed analysis, because proton signals in the spectra of [(*E*)-**4a**−**e**]·Hg^{2+} in MeCN-d_3 are substantially broadened. Comparison of the ^{1}H NMR spectra of (*E*)-**4c**·Mg^{2+}, (*E*)-**4c**·Pb^{2+}, shown in Figures 2 and 3, reveals that the chemical shifts of the H−C(b), H−C(5′) and H−C(6′) hydrogen atoms in (*E*)-**4c**·Pb^{2+} are somewhat upfield relative to the same hydrogen atoms in (*E*)-**4c**·Mg^{2+}. These shifts suggest that [(*E*)-**4c**]·Pb^{2+} exists, in part, as a dimeric complex in which π-electron circulation in opposing aromatic and C=C

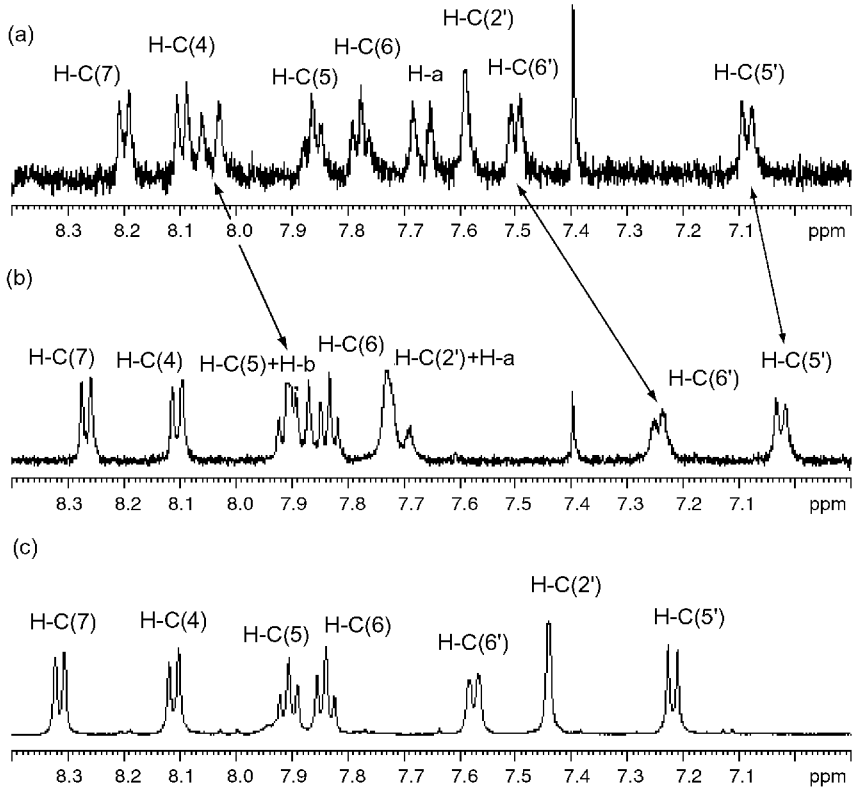

Figure 2. ^{1}H NMR spectra (aromatic part) of complexes (*E*)-**4c**·Mg^{2+} (a), (*E*)-**4c**·Pb^{2+} (b) and cyclobutane **5** (c) ($C = 0.005$ M) in MeCN-d_3 at 50 °C.

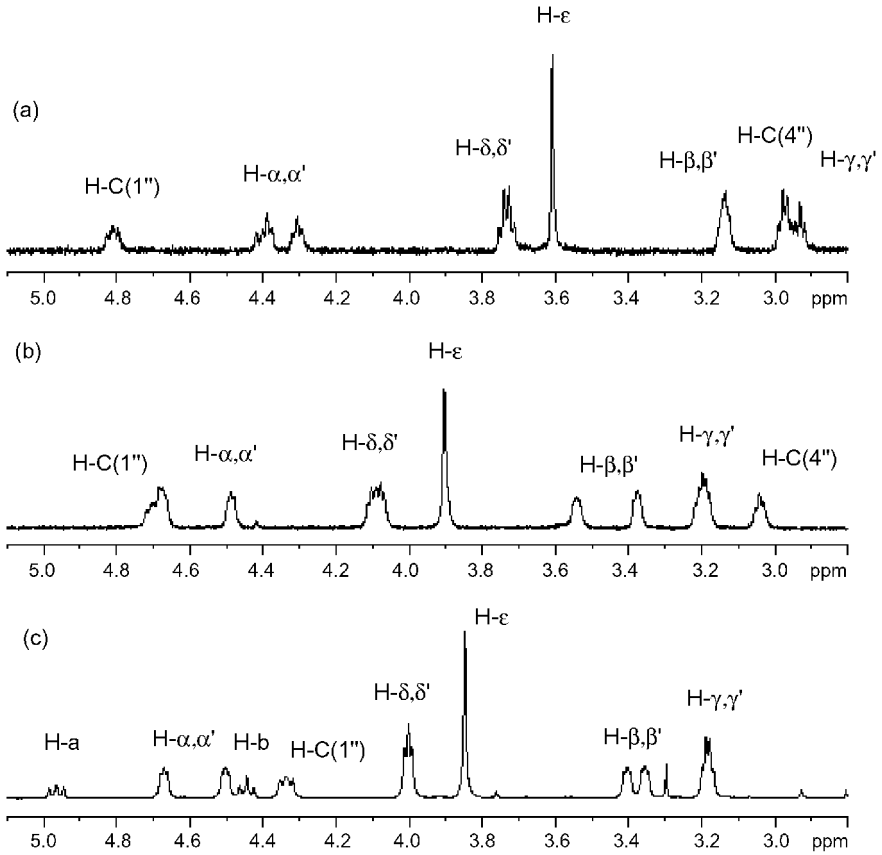

Figure 3. ^{1}H NMR spectra (aliphatic part) of complexes (*E*)-**4c**·Mg^{2+}(a), (*E*)-**4c**·Pb^{2+} (b) and cyclobutane **5** (c) (C = 0.005 M) in MeCN-d_3 at 50 °C.

SCHEME 4

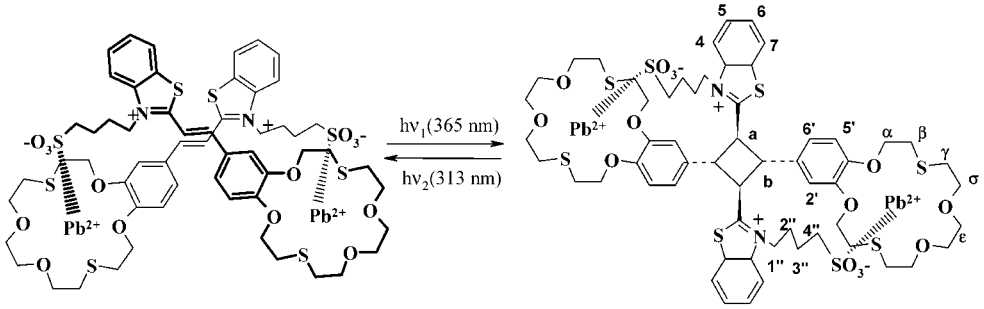

double bond moieties causes net deshielding in the H−C(b), H−C(5′) and H−C(6′) protons. Examination of molecular models of potential structures for dimeric complexes of (*E*)-**4c**·Pb^{2+} leads to a preference for the anti-"head-to-tail" configuration with crossed relationship of the (*E*)-**4c** ligands as shown in Scheme 4. The analogous structural assignment was made on theoretical grounds for dimeric complexes between (*E*)-CSDs containing oxygen crown ether moieties and Mg^{2+}.[28−31]

Spontaneous assembly leads to dimeric complexes whose architecture controls ligand photodimerization, and accounts for the stereospecific formation of cyclobutanes containing thiacrown ether moieties from the (*E*)-**4** CSDs. Accordingly, irradiation of the complexed forms of (*E*)-**4a**−**d** at 436 nm leads to *E*-CSD consumption in competition with the much faster $E \leftrightarrows Z$ photoisomerization. Because the latter reaction is reversible, prolonged irradiation at 365 nm of solutions containing (*E*)-**4a**−**d** in the presence of $Hg(ClO_4)_2$ or $Pb(ClO_4)_2$ leads to nearly complete loss of the CSDs. The UV spectrum of the [2+2]-photocycloadduct **5** obtained from the irradiation of a solution of **4c** in the presence of $Pb(ClO_4)_2$ is shown in Figure 4. Irradiation of CSDs **4a**−**d** under the same conditions but in the absence of the metal cation leads to no PCA. Similarly irradiated, CSDs **3a**−**e**, and **4e** undergo no photocycloaddition in the presence or in the absence of metal cations.

The single PCA obtained by irradiating *E*-**4c** in the presence of either Pb^{2+} or Hg^{2+} was assigned the cyclobutane structure **5** (Scheme 5), on the basis of its COSY and NOESY 2D ^{1}H NMR spectra and by comparison with available ^{1}H NMR spectral data for analogous cyclobutanes from the benzothiazole CSD series.[28−31] The olefinic protons H−a and H−b, seen as overlapping doublets, $^3J_{trans}$ = 15.6 Hz, in the spectrum of the (*E*)-**4c**/Pb^{2+} complex, Figures 2b are replaced by the cyclobutane

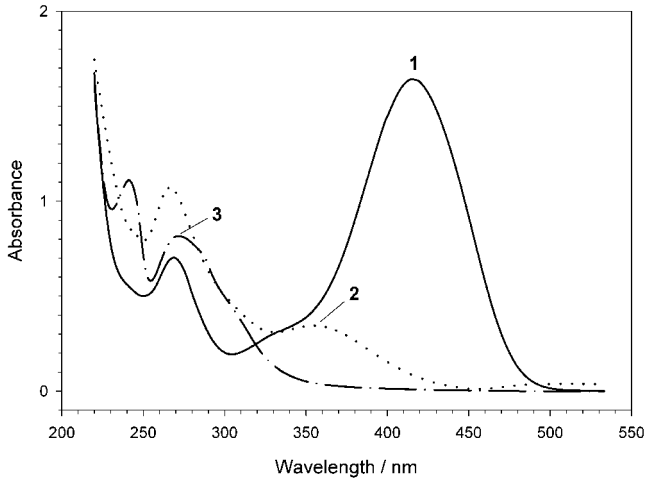

Figure 4. UV−vis absorption spectra of complexes of **4c** with $Pb(ClO_4)_2$ in MeCN ([**4c**] = 4×10^{-5} M, [Pb^{2+}] = 7×10^{-5} M): [(*E*)-**4c**]·Pb^{2+} (1), [(*Z*)-**4c**]·Pb^{2+} (2), PCA **5** (3).

SCHEME 5

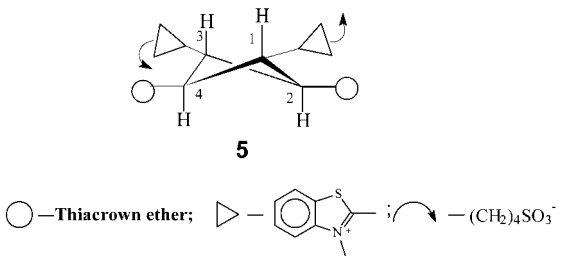

ring protons H−a and H−b in the ^{1}H NMR spectrum of **5**, responsible for the two triplets at 4.44 and 4.98 ppm, $^3J_{trans}$ = 9.6 Hz (an A_2B_2 type spin−spin coupling pattern), Figure 3c. The equatorial orientation of the substituents in **5**, is consistent with the prediction of a coupling constant of 10.75 Hz for the cyclobutane protons of the analogous structure of 1,2,3,4-tetraphenylcyclobutane.[32]

Although UV−vis and ^{1}H NMR spectra show that the same PCA **5** is obtained by irradiation of (*E*)-**4c** in the presence of either Hg^{2+} or Pb^{2+}, the quantum yield of photodimer formation is substantially more efficient in the presence of Pb^{2+} than in the presence of Hg^{2+} (Table 3). This is surprising in view of the much smaller value of the stability constant of the (*E*)-**4c**·Pb^{2+} complex, Table 2. It is not known at present whether the quantum yield difference is due to (a) a more favorable orientation of the CSD units in the Pb^{2+} dimeric complex, (b) a longer excited-state lifetime for the Pb^{2+} dimeric complex, and/or (c) a higher dimeric complex concentration as a result of stronger Pb^{2+}/SO_3^- than Hg^{2+}/SO_3^- coordination bonds.

Exposure of (*E*)-**4a**−**d** MeCN solutions in the presence of Hg^{2+} or Pb^{2+} to visible light, leads to UV−vis spectral changes typical of $E \leftrightarrows Z$ isomerization. The behavior of complexes [(*E*)-**4a**,**b**,**d**]·Hg^{2+} is analogous to that previously described for the (*E*)-**4c**·Hg^{2+} complex, whose *Z*-isomer is anion-"capped".[19] Observed LAB shifts of 50−70 nm on complexation of (*Z*)-**4a**,**b**,**d** with Hg^{2+} are consistent with diminished conjugation between the three moieties comprising the CSD chromophore, due to the pronounced departure from planarity that accompanies formation of anion-"capped" complexes. Accordingly, complexes [(*Z*)-**4a**,**b**,**d**]·Hg^{2+} are assigned anion-"capped" structures (Scheme 3). Enhanced stability due to intramolecular coordination in the anion-"capped" [(*Z*)-**4a**,**b**,**d**]·Hg^{2+} complexes is reflected in the stability constants in Table 2 (K_Z/K_E equals 10 for **4c**·Hg^{2+} and 15 for **4c**·Pb^{2+}) and causes sharp decelerations of their dark $Z \rightarrow E$ isomerizations (Scheme 3). The saturated coordination capacity that prevents dimeric complex formation from CSD (*E*)-**4e**·Hg^{2+} also explains why its *Z* isomer does not form an anion-"capped" complex. The *Z* isomers of CSDs (*E*)-**4a**−**d** also form anion-"capped" complexes with Pb^{2+} (the spectra in Figure 4 are typical), however, no such spectral evidence could be found when Cd^{2+}, Ni^{2+} or Zn^{2+} was substituted for Pb^{2+}. As expected, based on the theory of "hard" and "soft" acids and bases, the strength of the coordination bond between Cd^{2+}, Ni^{2+}, or Zn^{2+} and the SO_3- group appears to be too small to stabilize the *Z* isomer.

Quantum Yield Interpretation. The quantum yields of the competing photochemical reactions of dyes *E*-**4a**−**e** in the presence of $Hg(ClO_4)_2$ in acetonitrile are listed in Table 3. Sums of quantum yields of $Z \leftrightarrows E$ photoisomerization in the two directions are close to unity, consistent with the involvement of common excited state intermediates, and are relatively insensitive to the identity of the crown ether moiety. In contrast, the efficiency of PCA formation depends strongly on the size and on the S/O ratio of the crown ether moiety. The effective quantum yield of PCA formation, ϕ_{PCA}, attains a maximum value of 2.8×10^{-3} for **4b** and decreases more than 20-fold when the size of the crown ether cavity is either decreased or increased by a CH_2CH_2O unit, $\phi_{PCA} = 1.3 \times 10^{-4}$ for **4a** and **4c**. A further decrease in ϕ_{PCA} is observed when the crown ether cavity is increased by adding a second CH_2CH_2O unit, $\phi_{PCA} = 0.79 \times 10^{-4}$ for **4d**. Actual ϕ_{PCA} values should be considerably larger than effective values, because the dimeric complexes absorb only small fractions of the total absorbed excitation light intensity (see next paragraph). The role of the identity of the metal cation in controlling the efficiency of the photodimerization remains to be established. Substitution of two S atoms for two O atoms in the crown ether moiety of the CSD (compare **4c** with **4e** in Table 3) essentially eliminates PCA formation as a competing reaction. It is likely that in **4e** saturation of the coordination capacity of Hg^{2+} by the two additional Hg^{2+}/S bonds attenuates the interaction of Hg^{2+} with the sulfonate group, markedly diminishing the contribution of dimeric complex formation. PCA formation is photochemically reversible. Irradiation at 313 nm of a solution of **5** in MeCN containing $Hg(ClO_4)_2$, causes photocycloreversion with a quantum yield of 4×10^{-3}, leading to a photostationary state (PSS) which consists of **5** and *E*- and *Z*-**4c**.

The concentration dependence of effective PCA formation quantum yields was explored for the (*E*)-**4c**/$Pb(ClO_4)_2$ system in MeCN, Table 4. In view of the magnitude of log K_E for 1:1 complex formation, Table 2, essentially all of the ligand is present as a complex with Pb^{2+} for all concentration combinations in Table 4. This is consistent with the observation that the PSS composition for a total ligand concentration of 1.0×10^{-5} M is invariant for a 50-fold change in the concentration of Pb^{2+}. Ion-capping in the (*Z*)-**4c**·Pb^{2+} complex ensures that this condition will hold at the *E*/*Z* PSS for which the φ_{PCA} values apply. Formation of the 2:2 complex is reflected in the increase in φ_{PCA} and in an accompanying decrease of the *Z* content of the PSS with increasing [**4c**], since structural and electronic constraints in the 2:2 complex are expected to inhibit $E \rightarrow Z$ photoisomerization. An approximate interpretation of the φ_{PCA} values in Table 4 can be based on the assumptions that (*E*)-**4c**·Pb^{2+} and [(*E*)-**4c**·Pb^{2+}]$_2$ complexes have the same absorbance at 365 nm, and that no $E \rightarrow Z$ photoisomerization occurs

in the latter. The minimum number of required steps is as follows

$$(E)\text{-}\mathbf{4c}\cdot Pb^{2+} \xrightarrow{h\nu} (E)\text{-}\mathbf{4c}\cdot Pb^{2+}* \quad (4)$$

$$(E)\text{-}\mathbf{4c}\cdot Pb^{2+}* \rightarrow (p)\text{-}\mathbf{4c}\cdot Pb^{2+}* \quad (5)$$

$$(p)\text{-}\mathbf{4c}\cdot Pb^{2+}* \rightarrow \alpha(E)\text{-}\mathbf{4c}\cdot Pb^{2+} + (1-\alpha)(Z)\text{-}\mathbf{4c}\cdot Pb^{2+} \quad (6)$$

$$(Z)\text{-}\mathbf{4c}\cdot Pb^{2+} \xrightarrow{h\nu} (Z)\text{-}\mathbf{4c}\cdot Pb^{2+}* \quad (7)$$

$$(Z)\text{-}\mathbf{4c}\cdot Pb^{2+}* \rightarrow (p)\text{-}\mathbf{4c}\cdot Pb^{2+}* \quad (8)$$

$$2(E)\text{-}\mathbf{4c}\cdot Pb^{2+} \rightleftarrows [(E)\text{-}\mathbf{4c}\cdot Pb^{2+}]_2 \quad (9)$$

$$[(E)\text{-}\mathbf{4c}\cdot Pb^{2+}]_2 \xrightarrow{h\nu} [(E)\text{-}\mathbf{4c}\cdot Pb^{2+}]_2* \quad (10)$$

$$[(E)\text{-}\mathbf{4c}\cdot Pb^{2+}]_2* \rightarrow \beta PCA + (1-\beta)[(E)\text{-}\mathbf{4c}\cdot Pb^{2+}]_2 \quad (11)$$

$$[(E)\text{-}\mathbf{4c}\cdot Pb^{2+}]_2* + Pb^{2+} \rightarrow [(E)\text{-}\mathbf{4c}\cdot Pb^{2+}]_2 + Pb^{2+} \quad (12)$$

Neglecting the small fluorescence quantum yield and eqs 9−12, at relatively low concentrations, this mechanism predicts that the *E*/*Z* PSS ratio will be given by

$$[(E)\text{-}\mathbf{4c}\cdot Pb^{2+}]/[(Z)\text{-}\mathbf{4c}\cdot Pb^{2+}] = (\epsilon_c/\epsilon_t)[\alpha/(1-\alpha)] \quad (13)$$

where ϵ_c/ϵ_t is the ratio of the molar absorptivities of the *E* and *Z* 1:1 complexes at 365 nm. Extrapolation based on the PSS values for $[Pb^{2+}] = 1.0 \times 10^{-3}$ M in Table 4 gives an *E*/*Z* PSS ratio of 0.513 at infinite [**4c**·Pb^{2+}] dilution. Strictly speaking, due to the competing formation of **5**, the *E*/*Z* ratios are quasi-photostationary states (Q-PSSs). Use of the PSS designation is justified, however, because the φ_{PCA} values are relatively low. By attributing all increase in the *E*/*Z* PSS ratio with increasing [**4c**·Pb^{2+}] to formation of 2:2 complex, the value of K_2, the equilibrium constant for eq 9, is estimated as $(7.8 \pm 0.2) \times 10^3$ M^{-1} for the two lowest [**4c**·Pb^{2+}] values for $[Pb^{2+}] = 1.0 \times 10^{-3}$ M. The concentrations of *E* and *Z* 1:1 complexes and of *E* 2:2 complex at the PSS calculated with this K_2, together with the spectra in Figure 4, give estimates of 4.4 and 10.1% as the excitation light absorbed by the [(*E*)-**4c**·Pb^{2+}]$_2$ complex for the first two rows in Table 4. Accordingly, the corresponding φ_{PCA} values in Table 4, can be adjusted upward from 0.289×10^{-3} and 0.708×10^{-3} to 6.5×10^{-3} and 7.0×10^{-3}, respectively. However, even these adjusted values probably underestimate the intrinsic fraction of excited [(*E*)-**4c**·Pb^{2+}]$_2$ complexes that gives the dimer because they do not account for the fact that a 50-fold increase in $[Pb^{2+}]$ at constant [**4c**·Pb^{2+}] $= 1.0 \times 10^{-5}$ M diminishes the effective φ_{PCA} value from 0.818×10^{-3} to 0.289×10^{-3}. Equation 12 could provide an explanation for the effect of Pb^{2+} if the lifetime of [(*E*)-**4c**·Pb^{2+}]$_2$* were sufficiently long. A more attractive alternative explanation is that competing association of (*E*)-**4c**·Pb^{2+} with Pb^{2+} at the alkyl sulfonate side chain blocks formation of [(*E*)-**4c**·Pb^{2+}]$_2$, the PCA precursor, Scheme 6. Product quantum yields were measured in the presence of air because oxygen does not quench the weak fluorescences of **4c** and [**4c**·Pb^{2+}], $\varphi_f = 0.012$ and 0.013, respectively, for $\lambda_{exc} = 365$ nm. The inferred short singlet excited-state lifetime of (*E*)-**4c**·Pb^{2+} also precludes formation of **5** via diffusional encounters of ground and singlet excited states of (*E*)-**4c**·Pb^{2+}.

The above mechanism does not account for the apparent leveling off of PSS and effective φ_{PCA} values at the highest **4c** concentration in Table 4. A weakness of the above interpretation is that it assumes the same absorbance for (*E*)-**4c**·Pb^{2+} and [(*E*)-**4c**·Pb^{2+}]$_2$ complexes at 365 nm, thus neglecting the observed concentration dependent spectral shifts. More information is required before a more quantitative interpretation of the φ_{PCA} values in Table 4 can be presented. Scheme 6 gives a tentative interpretation of the concentration dependence of φ_{PCA}, which is consistent with the changes in the UV−vis spectra. It includes the possibility that $E \rightarrow Z$ photoisomerization, which may be entirely suppressed in the 2:2 complex, is not suppressed in higher aggregates.

SCHEME 6

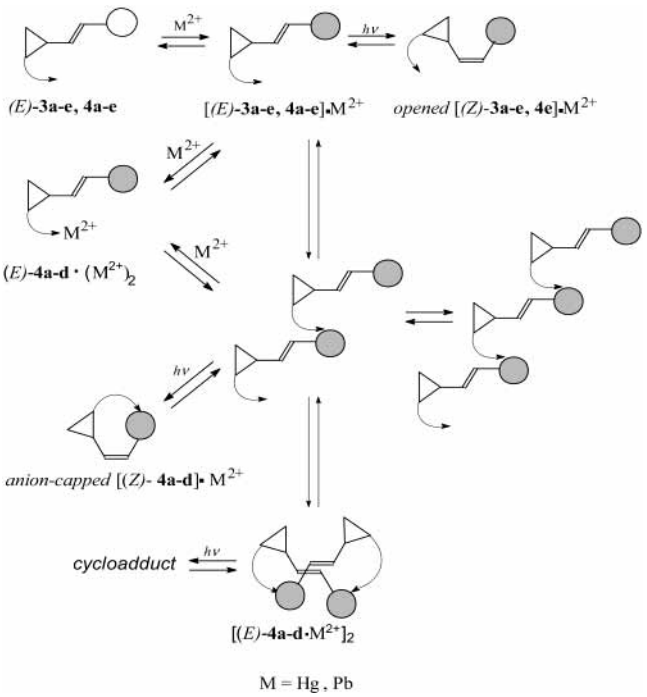

Summary

The photochemical processes observed in this work on irradiation of acetonitrile solutions of CSDs (*E*)-**3a**−**e** and **4a**−**e** in the presence of metal cations are summarized in Scheme 6. Incorporation of the metal cations into the crown ether cavity of the CSDs leads to formation of 1:1 ligand to metal cation complexes that undergo reversible $Z \leftrightarrows E$ photoisomerization. The Hg^{2+} and Pb^{2+} complexes of the *Z* isomers of betaine dyes **4a**−**d** show unusual stability because they assume anion-"capped" structures through the interaction of the *N*-butylsulfonate group with the metal cation in the crown ether cavity. The *E* isomers of the complexes of CSDs **4a**−**d** with the soft metal cations Hg^{2+} or Pb^{2+} undergo further self-organization to yield equilibrium mixtures with dimeric complexes having *anti*-head-to-tail CSD orientation. Prolonged irradiation of solutions containing dimeric complexes leads to excitation wavelength-dependent reversible stereoselective formation of cyclobutane photoproducts. It is noteworthy that metal cation complexes of **3a**−**e**, which, lacking the *N*-alkylsulfonate group, undergo neither anion-"capped" *Z* complex formation nor dimeric *E* complex formation, fail to give [2+2]-photocycloadducts. Similarly, no photocycloadducts are observed on irradiation of complexes of the "soft" metal cations Hg^{2+} and Pb^{2+} with **4e** because the four S atoms in the crown ether cavity saturate the coordination capacity of the metal cations and render the *N*-alkylsulfonate group ineffective, both with respect to

anion-"capped" *Z* complex formation and with respect to self-organization of the *E* isomer into dimeric complexes.

This work demonstrates that, with proper structural design of the thiacrown ether moiety that is incorporated in the photochromic system, both light-modulated metal selectivity and highly specific aggregation leading to stereospecific photodimerization can be achieved. Improved understanding of such factors is an essential first step toward construction of novel multifunctional systems with useful properties.

Experimental Part

Analytical Methods. The ^{1}H NMR spectra were recorded at 323 K on a Bruker DRX-500 spectrometer operating at 500.13 MHz. The chemical shifts were measured with an accuracy of 0.01 ppm, and spin−spin coupling constants were determined with an accuracy of 0.1 Hz. The sample of the cyclobutane derivative obtained from [(*E*-**4c**)·Pb^{2+}]$_2$ was dissolved in CD_3CN with addition of D_2O. The COSY and NOESY 2D spectra were recorded using the standard Bruker pulse sequences (cosy45, cosygs, noesytp, roesyprtp) and processed using the XWINNMR program. The mixing time for the NOESY spectra was 700 ms, the delay between scans was 2 s, and the number of scans per experiment was 32. Totals of 512 f1 points and 2048 f2 points were accumulated. The signals in the ^{1}H NMR spectra of [(*E*-**4c**)]·Mg^{2+}, [(*E*-**4c**)]·Pb^{2+}, and the cyclobutane derivative obtained from [(*E*-**4c**)·Pb^{2+}]$_2$ were assigned based on the NOEs obtained in the NOESY experiments.

Spectroscopic Measurements. UV−vis spectra were recorded with a Specord-M40 spectrophotometer. Preparation of solutions and all measurements were carried out in red light. Steady-state fluorescence spectra were recorded on a Shimadzu RF-5000 spectrofluorometer. The fluorescence quantum yields of ligand and complex in air-saturated acetonitrile were determined at 20 ± 1 °C relative to fluorescein in 0.01 M NaOH in water ($\varphi_f = 0.92$)[33] with excitation at 365 nm. Quantum yields were based on integrated uncorrected fluorescence spectra.

Photochemical Measurements. Photochemical experiments were carried out by exposing air-saturated acetonitrile solutions of CSD/cation mixtures at 20 ± 1 °C to the filtered light of a DRK-120 mercury lamp. Individual lines of this lamp (313, 365, and 436 nm) were isolated with the use of glass filters. Quantum yields for $E \rightarrow Z$ photoisomerization (ϕ_{t-c}) and PCA (ϕ_{PCA}) for **4a**−**e** and their complexes with $Hg(ClO_4)_2$ or $Pb(ClO_4)_2$ were determined upon irradiation of solutions at 365 nm. Ferrioxalate, 0.006 M, was employed as the actinometer in the quantum yield measurements.[34]

Polarographic Procedures. Polarographic experiments were carried out in acetonitrile with a Model 263a potentiostat/galvanostat (EG&G Princeton Applied Research) and a Model 303A dropping-mercury electrode (DME) (EG&G Princeton Applied Research). Potentials were measured vs an Ag/(0.010 M $AgNO_3$ in acetonitrile) electrode, and the salt bridge solution was 0.1 M Et_4NClO_4 in acetonitrile. This reference electrode was kept in contact with the testing solution via a Vycor frit supplied by EG&G Princeton Applied Research. The method of differential-pulse polarography was used for all experiments. The potential scanning rate was 2 mV/s and the dropping time of the DME was 1 s. The supporting electrolyte was 0.1 M Et_4NClO_4. Values of the half-wave potentials of Hg anodic waves were found from the individual polarograms. All experiments were performed at 20 °C under an argon atmosphere.

Materials. Unless stated otherwise, reagents and solvents were obtained from commercial sources and used as received. The syntheses of **1a**,**b**, **2a**−**e** and CSDs **3c**,**4c** used were as previously described.[14−19] the general procedure for the syntheses of the CSDs is given below.

Syntheses of CSDs **3a**−**e**, **4a**−**e**: Dry pyridine (0.3 mL) was added to a solution of 0.11 mmol of heterocyclic salt **1a**,**b** and 0.12 mmol of **2a**−**e** in anhydrous ethanol (2 mL). The mixture was refluxed for 17 h and concentrated in vacuo. The residue was washed with benzene and extracted by heating with 35 mL of methanol, and the methanol solution was cooled to 0 °C. The precipitates, (*E*)-**3a**−**e** and **4a**−**e**, formed after 1 h and were isolated by filtration.

2-[(*E*)-2-(2,3,5,6,8,9-Hexahydro-1,10,4,7-benzodioxadithiacyclododecin-12-yl)-1-ethenyl]-3-methyl-1,3-benzothiazol-3-ium perchlorate (3a): Yield 76%; mp 148−151 °C; ^{1}H NMR (CD_3CN) δ 2.99 (*m*, 2 CH_2S); 3.04 (*s*, 2 CH_2S); 4.25 (*s*, CH_3); 4.43 (*m*, CH_2OAr); 4.48 (*m*, CH_2OAr); 7.05 (*d*, J = 8.3, H−C(5′)); 7.48 (*d*, J = 8.3, H−C(6′)); 7.49 (*s*, H−C(2′)); 7.56 (*d*, $^3J_{trans}$ = 15.7, H−a); 7.78, 7.87 (*2 m*, H−C(5), H−C(6)); 8.04 (*d*, J^3_{trans} = 15.7, H−b); 8.02, 8.20 (*2 d*, J = 8.5, H−C(4), J = 8.0, H−C(7)). Anal. Calcd (%) for $C_{22}H_{24}ClNO_6S_3 \cdot H_2O$: C, 54.45; H, 5.83; N, 2.42. Found (%): C, 54.29; H, 5.69; N, 2.56.

2-[(*E*)-2-(2,3,5,6,8,9-Hexahydro-1,10,4,7-benzodioxadithiacyclododecin-12-yl)-1-ethenyl]-3-(4-sulfobutyl)-1,3-benzothiazol-3-ium betaine (4a): Yield 80%; mp 262−264 °C; ^{1}H NMR (DMSO-d_6) δ 1.93 (*m*, $CH_2CH_2CH_2CH_2SO_3^-$); 2.14 (*m*, $CH_2CH_2CH_2CH_2SO_3^-$); 2.68 (*t*, J = 6.3, $CH_2CH_2CH_2CH_2SO_3^-$); 2.95 (*m*, 2 CH_2S); 3.01 (*s*, 2 CH_2S); 4.43 (*m*, CH_2OAr); 4.59 (*m*, CH_2OAr); 4.96 (*m*, $CH_2CH_2CH_2CH_2SO_3^-$); 7.09 (*d*, J = 8.3, H−C(5′)); 7.54 (*d*, J = 8.3, H−C(6′)); 7.76, 7.84 (*2 m*, H−C(5), H−C(6)); 8.01 (*s*, H−C(2′)); 8.11 (*d*, $^3J_{trans}$ = 15.7, H−a); 8.20 (*d*, $^3J_{trans}$ = 15.7, H−b); 8.30, 8.36 (*2 d*, J = 8.8, H−C(4)), J = 8.1, H−C(7)). Anal. Calcd (%) for $C_{25}H_{29}NO_5S_4 \cdot H_2O$: C, 52.70; H, 5.48; N, 2.46. Found (%): C, 53.27; H, 5.32; N, 2.46.

3-Methyl-2-[(*E*)-2-(2,3,5,6,8,9,11,12-octahydro-1,7,13,4,10-benzotrioxadithia-cyclopentadecin-15-yl)-1-ethenyl]-1,3-benzothiazol-3-ium perchlorate (3b): Yield 71%; mp 129−130 °C; ^{1}H NMR (CD_3CN): 2.95 (*m*, 2 CH_2S); 3.10 (*m*, CH_2S); 3.13 (*m*, CH_2S); 3.78 (*m*, 2 CH_2O); 4.24 (*s*, CH_3); 4.35 (*m*, CH_2OAr); 4.37 (*m*, CH_2OAr); 7.09 (*d*, J = 8.8, H−C(5′)); 7.49 (*m*, H−C(6′), H−C(2′)); 7.56 (*d*, $^3J_{trans}$ = 15.7, H−a); 7.78, 7.87 (*2 m*, H−C(5), H−C(6)); 8.02, 8.20 (*2 d*, J = 8.0, H−C(7), H−C(4)); 8.05 (*d*, $^3J_{trans}$ = 15.7, H−b). Anal. Calcd (%) for $C_{24}H_{28}ClNO_7S_3$: C, 50.21; H, 4.92; N, 2.44. Found (%): C, 50.24; H, 4.93; N, 2.64.

2-[(*E*)-2-(2,3,5,6,8,9,11,12-Octahydro-1,7,13,4,10-benzotrioxadithiacyclopentadecin-15-yl)-1-ethenyl]-3-(4-sulfobutyl)-1,3-benzothiazol-3-ium betaine (4b): Yield 65%; mp 270−272 °C; ^{1}H NMR (DMSO- d_6) δ 1.91 (*m*, $CH_2CH_2CH_2CH_2SO_3^-$); 2.11 (*m*, $CH_2CH_2CH_2CH_2SO_3^-$); 2.67 (*tr*, J = 6.5, $CH_2CH_2CH_2CH_2SO_3^-$); 2.90 (*m*, 2 CH_2S); 3.07 (*m*, 2 CH_2S); 3.73 (*m*, 2 CH_2O); 4.33 (*m*, CH_2OAr); 4.45 (*m*, CH_2OAr); 4.95 (*m*, $CH_2CH_2CH_2CH_2SO_3^-$); 7.12 (*d*, J = 8.3, H−C(5′)); 7.56 (*d*, J = 8.3, H−C(6′)); 7.76, 7.84 (*2m*, H−C(5), H−C(6)); 7.96 (*s*, H−C(2′)); 8.11 (*d*, $^3J_{trans}$ = 15.6, H−a); 8.19 (*d*, $^3J_{trans}$ = 15.6, H−b); 8.30, 8.37 (*2 d*, J = 8.5, H−C(4), J = 8.0, H−C(7)). Anal. Calcd (%) for $C_{27}H_{33}NO_6S_4$: C, 54.43; H, 5.58; N, 2.35. Found (%): C, 54.31; H, 5.63; N, 2.37.

2-[(*E*)-2-(2,3,5,6,8,9,11,12,14,15,17,18-Dodecahydro-1,7,10,-13,19,4,16-benzopentaoxa-dithiacyclohenicosin-21-yl)-1-ethenyl]-3-methyl-1,3-benzothiazol-3-ium perchlorate (3d): Yield 55%; mp 198−201 °C; ^{1}H NMR (CD_3CN) δ 2.93 (*m*, 2 CH_2S); 3.07 (*m*, 2 CH_2S); 3.62 (*s*, 4 CH_2O); 3.75 (*m*, 2 CH_2O); 4.26 (*s*, CH_3); 4.34 (*m*, 2 CH_2OAr); 7.12 (*d*, J = 8.3, H−C(5′)); 7.50 (*d*, J = 8.3, H−C(6′)); 7.52 (*s*, H−C(2′)); 7.56 (*d*, $^3J_{trans}$ = 15.7, H−a,); 7.79, 7.88 (*2 m*, H−C(5), H−C(6)); 8.03, 8.20

(*2 d*, J = 8.4, H−C(4), J = 8.0, H−C(7)); 8.04 (*d*, J = 15.7, H−b). Anal. Calcd (%) for $C_{28}H_{36}ClNO_9S_3$: C, 50.78; H, 5.48; N, 2.12. Found (%): C, 50.60; H, 5.67; N, 2.07.

2-[(*E*)-2-(2,3,5,6,8,9,11,12,14,15,17,18-Dodecahydro-1,7,10,-13,19,4,16-benzopentaoxa-dithiacyclohenicosin-21-yl)-1-ethenyl]-3-(4-sulfobutyl)-1,3-benzothiazol-3-ium betaine (4d): Yield 62%; mp 267−269 °C; ^{1}H NMR (CD_3CN-D_2O) δ 1.97 (*m*, CH_2CH_2*CH_2*$CH_2SO_3^-$); 2.09 (*m*, CH_2*CH_2*$CH_2CH_2SO_3^-$); 2.89 (*m*, 2 *CH_2*S, $CH_2CH_2CH_2$*CH_2*SO_3^-); 3.01 (*m*, 2 *CH_2*S); 3.59 (*s*, 4 *CH_2*O); 3.71 (*m*, 2 *CH_2*O); 4.26 (*t*, J = 6.2, *CH_2*-OAr,); 4.33 (*t*, J = 6.1, *CH_2*OAr,); 4.78 (*m*, *CH_2*CH_2CH_2-$CH_2SO_3^-$); 7.06 (*d*, J = 8.5, H−C(5′)); 7.47 (*d*, J = 8.5, H−C(6′)); 7.55 (*s*, H−C(2′)); 7.66 (*d*, $^3J_{trans}$ = 15.6, H−a); 7.72, 7.83 (*2 m*, H−C(5), H−C(6)); 8.01 (*d*, J_{trans} = 15.6, H−b); 8.10, 8.14 (*2 d*, J = 8.5, H−C(4), J = 8.2, H−C(7)). Anal. Calcd (%) for $C_{31}H_{41}NO_8S_4$·0.5H_2O: C, 53.73; H, 6.11; N, 2.02. Found (%): C, 53.66; H, 6.01; N, 1.84.

2-[(*E*)-2-(2,3,5,6,8,9,11,12,14,15-Decahydro-1,16,4,7,10,13-benzodioxatetrathia-cyclooctadecin-18-yl)-1-ethenyl]-3-methyl-1,3-benzothiazol-3-ium perchlorate (3e): Yield 60%; mp 186−188 °C; ^{1}H NMR (DMSO-d_6) δ 2.88 (*m*, 3 *CH_2*S); 3.02 (*m*, 3 *CH_2*S); 3.10 (*t*, J = 4.7, *CH_2*S); 3.14 (*t*, J = 4.8, *CH_2*S); 4.35 (*m*, *CH_3*, 2 *CH_2*OAr); 7.18 (*d*, J = 8.5, H−C(5′)); 7.64 (*d*, J = 8.5, H−C(6′)); 7.72 (*s*, H−C(2′)); 7.78, 7.87 (*2 m*, H−C(5), H−C(6)); 7.90 (*d*, $^3J_{trans}$ = 15.7, H−a); 8.16 (*d*, $^3J_{trans}$ = 15.7, H−b); 8.22, 8.40 (*2 d*, J = 8.4, H−C(4), J = 8.1, H−C(7)). Anal. Calcd (%) for $C_{26}H_{32}ClNO_6S_5$: C, 48.02; H, 4.96; N, 2.15. Found (%): C, 48.18; H, 5.07; N, 2.37.

2-[(*E*)-2-(2,3,5,6,8,9,11,12,14,15-Decahydro-1,16,4,7,10,13-benzodioxatetrathia-cyclooctadecin-18-yl)-1-ethenyl]-3-(4-sulfobutyl)-1,3-benzothiazol-3-ium betaine (4e)): Yield 36%; mp 262−264 °C; ^{1}H NMR (DMSO-d_6) δ 1.93 (*m*, CH_2CH_2*CH_2*-$CH_2SO_3^-$); 2.14 (*m*, CH_2*$CH_2CH_2CH_2SO_3^-$); 2.68 (*t*, J = 6.5, $CH_2CH_2CH_2$*CH_2*SO_3^-); 2.88 (*m*, 3 *CH_2*S); 3.02 (*m*, 3 *CH_2*S); 3.10 (*m*, 2 *CH_2*S); 4.38 (*t*, J = 4.9, *CH_2*OAr,); 4.51 (*tr*, J = 4.9, *CH_2*OAr,); 4.97 (*m*, *CH_2*$CH_2CH_2CH_2SO_3^-$); 7.13 (*d*, J = 8.4, H−C(5′)); 7.56 (*d*, J = 8.4, H−C(6′)); 7.76, 7.84 (*2 m*, H−C(5), H−C(6)); 7.98 (*s*, H−C(2′)); 8.10 (*d*, $^3J_{trans}$ = 15.6, H−a); 8.21 (*d*, $^3J_{trans}$ = 15.6, H−b); 8.30, 8.36 (*2 d*, J = 8.5, H−C(4), J = 8.1, H−C(7)). Anal. Calcd (%) for $C_{29}H_{37}NO_5S_6$·1.5H_2O: C, 49.83; H, 5.77; N, 2.00. Found (%): C, 49.72; H, 5.42; N, 1.77.

Synthesis of the Cyclobutane PCA 5. A solution of dye **4c** (0.01 mmol) and $Pb(ClO_4)_2$ (0.0125 mmol) in dry MeCN (5 mL) was irradiated with light of a DRK-120 mercury lamp at λ = 365 nm for several hours. When the dye was wholly consumed (monitored by UV−vis spectroscopy), MeCN was evaporated in vacuo. The uncomplexed form of **5** was obtained upon addition of H_2O (5%, v/v) to the $Pb(ClO_4)_2$-containing MeCN solution of **5**, **2-{2,4-di(2,3,5,6,8,9,11,12,14,15-Decahydro-1,7,10,16,4,13-benzotetraoxadithia-cyclooctadecin-18-yl)-3-[3-(4-sulfobutyl)-1,3-benzothiazol-3-ium-2-yl]cyclobutyl}-3-(4-sulfobutyl)-1,3-benzothiazol-3-ium dibetaine:** ^{1}H NMR (MeCN-d_3-D_2O, 95:5) δ 1.10 (*m*, CH_2CH_2*CH_2*$CH_2SO_3^-$); 1.61 (*m*, CH_2*CH_2*$CH_2CH_2SO_3^-$); 2.46 (*m*, $CH_2CH_2CH_2$*CH_2*SO_3^-); 3.18 (*m*, 4 *CH_2*S); 3.35 (*m*, 2 *CH_2*S); 3.40 (*m*, 2 *CH_2*S); 3.85 (*s*, 4 *CH_2*O); 4.00 (*m*, 4 *CH_2*S); 4.33 (m, 4 H, *CH_2*CH_2CH_2-$CH_2SO_3^-$); 4.44 (*t*, 2 H−(C−b) $^3J_{H-C(b),H-C(a)}$ = 9.6) 4.50 (*m*, 2 *CH_2*OAr); 4.67 (*m*, 2 *CH_2*OAr); 4.96 (*t*, H−(C−a), $^3J_{H-C(a),H-C(b)}$ = 9.6)); 7.22 (*d*, 2 H−C(5′)); 7.44 (*s*, 2 H−C(2′)); 7.57 (*d*, 2 H−C(6)); 7.84 (*t*, 2 H−C(6)); 7.90 (*t*, 2 H−C(5)); 8.11 (*d*, 2 H−C(4)); 8.32 (*d*, 2 H−C(7)).

Acknowledgment. This work was carried out with the support of the Russian Foundation for Basic Research (Project Nos. 01-03-32757, 00-03-32159 and 02-03-33058), the U.S. Civilian Research and Development Foundation for the Independent States of the Former Soviet Union (CRDF, Grant No. RC2-2344-MO-02), and the INTAS (Grant 2001-0267). Work at Florida State University was supported in part by NSF Grant CHE-9985895.

References and Notes

(1) Mishra, A.; Behera, R. K.; Behera, P. K.; Mishra, B. K.; Behera, G. B. *Chem. Rev.* **2000**, *100*, 1973.
(2) Ke, W.; Xu, H.; Liu, X.; Luo, X. *Heterocycles* **2000**, *53*, 1821.
(3) Lëhr, H.-G.; Vögtle, F. *Acc. Chem. Res.* **1985**, *18*, 65.
(4) Takagi, M. In *Cation Binding by Macrocycles. Complexation of Cationic Species by Crown Ethers*; Inoue, Y., Gokel, G. W., Eds.; Marcel Dekker: New York, 1990; Chapter 11, p 465.
(5) Pietraszkiewicz, M. In *Comprehensive Supramolecular Chemistry*; Reinhoudt, D. N., Ed.; Pergamon: Oxford, U.K., 1996; Vol. 10, Chapter 10, p 225.
(6) De Silva, A. P.; Gunaratne, H. Q. N.; Gunnlaugsson, T.; Huxley, A. J. M.; McCoy, C. P.; Rademacher, J. T.; Rice, T. E. *Chem. Rev.* **1997**, *97*, 1515.
(7) Kimura, K. *Coord. Chem. Rev.* **1996**, *148*, 41.
(8) Valure, B.; Leray, I. *Coord. Chem. Rev.* **2000**, *205*, 3.
(9) Alfimov, M. V.; Gromov, S. P. In *Applied Fluorescence in Chemistry, Biology, and Medicine*; Rettig, W., Strehmel, B., Schrader, S., Seifert, H., Eds.; Springer-Verlag: Berlin, 1999; p 161.
(10) Humphry-Baker, R. *Angew. Chem.* **1979**, *91*, 669.
(11) Balzani, V.; Campagna, S.; Denti, G.; Juris, A.; Serroni, Sc.; Venturi, M. *Acc. Chem. Res.* **1998**, *31*, 26.
(12) Fedorova, O. A.; Gromov, S. P. In. *Targets in Heterocyclic Synthesis*; 2000; v.4.
(13) Gromov, S. P.; Alfimov, M. V. *Izv. Akad. Nauk, Ser. Khim.* **1997**, 641; *Russ. Chem. Bull.* **1997**, *46*, 611.
(14) Fedorova, O. A.; Vedernikov, A. I.; Gromov, S. P.; Yescheulova, O. V.; Tsapenko, P. V. *Izv. Akad. Nauk, Ser. Khim.* **2000**, 999; *Russ. Chem. Bull.* **2000**, *46*, 947.
(15) Alfimov, M. V.; Fedorov, Yu. V.; Fedorova, O. A.; Gromov, S. P.; Hester, R. E.; Lednev, I. K.; Moore, J. N.; Oleshko, V. P.; Vedernikov, A. I. *J. Chem. Soc., Perkin Trans. 2* **1996**, 1441.
(16) Alfimov, M. V.; Fedorov, Yu. V.; Fedorova, O. A.; Gromov, S. P.; Hester, R. E.; Lednev, I. K.; Moore, J. N.; Oleshko, V. P.; Vedernikov, A. I. *Spectrochim. Acta* **1997**, Part A *53*, 1853.
(17) Gromov, S. P.; Fedorova, O. A.; Vedernikov, A. I.; Fedorov, Yu. V.; Alfimov, M. V. *Izv. Akad. Nauk, Ser. Khim.* **1997**, 2213; *Russ. Chem. Bull.* **1997**, *46*, 2099.
(18) Alfimov, M. V.; Vedernikov, A. I.; Gromov, S. P.; Fedorov, Yu. V.; Fedorova, O. A. *Izv. Akad. Nauk, Ser. Khim.* **1997**, 1007; *Russ. Chem. Bull.* **1997**, *46*, 967.
(19) Alfimov, M. V.; Gromov, S. P.; Fedorova, O. A.; Vedernikov, A. I.; Churakov, A. V.; Kuz'mina, L. G.; Howard, J. A. K.; Bossmann, S.; Braun, A.; Woerner, M.; Sears, D. F., Jr.; Saltiel, J. *J. Am. Chem. Soc.* **1999**, *121*, 4992−5000.
(20) Bradshaw, J. S.; Hui, J. Y. K. *J. Heterocycl. Chem.* **1974**, *11*, 649.
(21) Kahn, O.; Morgestern-Badaru, I.; Audiere, J. P.; Lehn, J.-M.; Sullivan, S. A. *J. Am. Chem. Soc.* **1980**, *102*, 5935.
(22) Weber, E.; Vögtle, F. *Just. Lieb. Ann. Chem.* **1976**, 891.
(23) Bradshaw, J. S.; Stott, P. E. *Tetrahedron* **1980**, 461.
(24) Gans, P.; Sabatini, A.; Vacca, A. *Talanta* **1996**, *43*, 1739.
(25) Coetzee, J. F.; Campion, J. J.; Liberman, D. R. *Anal. Chem.* **1973**, *45*, 343.
(26) Coetzee, J. F.; Simon, J. M.; Bertozzi, R. J. *Anal. Chem.* **1969**, *41*, 766.
(27) Fischer, E. *J. Phys. Chem.* **1967**, *71*, 3704.
(28) Gromov, S. P.; Ushakov, E. N.; Fedorova, O. A.; Buevich, A. V.; Alfimov, M. V. *Izv. Akad. Nauk, Ser. Khim.* **1996**, 693; *Russ. Chem. Bull.* **1996**, *45*, 722.
(29) Gromov, S. P.; Fedorova, O. A.; Ushakov, E. N.; Baskin, I. I.; Lindeman, A. V.; Valysheva, E. V.; Balashova, T. A.; Arsenjev, A. S.; Alfimov, M. V. *Izv. Akad. Nauk, Ser. Khim.* **1998**, 99; *Russ. Chem. Bull.* **1998**, *47*, 97.
(30) Gromov, S. P.; Fedorova, O. A.; Ushakov, E. N.; Buevich, A. V.; Baskin, I. I.; Pershina, Y. V.; Eliasson, B.; Edlund, U.; Alfimov, M. V. *J. Chem. Soc., Perkin Trans. 2* **1999**, 1323.
(31) Gromov, S. P.; Fedorova, O. A.; Ushakov, E. N.; Buevich, A. V.; Alfimov, M. V. *Izv. Akad. Nauk, Ser. Khim.* **1995**, 2225; *Russ. Chem. Bull.* **1995**, *44*, 2131.
(32) Donati, D.; Fiorenza, M.; Fautoni, P. S. *J. Heterocycl. Chem.* **1979**, *16*, 253.
(33) Weber, G.; Teale, F. W. J. *Trans. Faraday Soc.* **1957**, *53*, 646.
(34) Parker, C. A. *Photoluminescence of Solutions*; Elsevier: Amsterdam, 1968; Ch.3.